AMERICAN SOCIETY FOR MICROBIOLOGY | Molecular and Cellular Biology®

RESEARCH ARTICLE

RNA-Binding Proteins PCBP1 and PCBP2 Are Critical Determinants of Murine Erythropoiesis

Xinjun Ji,[a] Anupama Jha,[b] Jesse Humenik,[a] Louis R. Ghanem,[c] Andrew Kromer,[a] Christopher Duncan-Lewis,[a] Elizabeth Traxler,[d] Mitchell J. Weiss,[e] Yoseph Barash,[a] Stephen A. Liebhaber[a,f]

[a]Department of Genetics, Perelman School of Medicine at the University of Pennsylvania, Philadelphia, Pennsylvania, USA
[b]Department of Computer and Information Science, School of Engineering and Applied Science at the University of Pennsylvania, Philadelphia, Pennsylvania, USA
[c]Gastroenterology, Hepatology and Nutrition Division, The Children's Hospital of Philadelphia, Philadelphia, Pennsylvania, USA
[d]Cell and Molecular Biology Graduate Group, Perelman School of Medicine at the University of Pennsylvania, Philadelphia, Pennsylvania, USA
[e]Department of Hematology, St. Jude Children's Research Hospital, Memphis, Tennessee, USA
[f]Department of Medicine, Perelman School of Medicine at the University of Pennsylvania, Philadelphia, Pennsylvania, USA

ABSTRACT We previously demonstrated that the two paralogous RNA-binding proteins PCBP1 and PCBP2 are individually essential for mouse development: *Pcbp1*-null embryos are peri-implantation lethal, while *Pcbp2*-null embryos lose viability at midgestation. Midgestation *Pcbp2*$^{-/-}$ embryos revealed a complex phenotype that included loss of certain hematopoietic determinants. Whether PCBP2 directly contributes to erythropoietic differentiation and whether PCBP1 has a role in this process remained undetermined. Here, we selectively inactivated the genes encoding these two RNA-binding proteins during differentiation of the erythroid lineage in the developing mouse embryo. Individual inactivation of either locus failed to impact viability or blood formation. However, combined inactivation of the two loci resulted in midgestational repression of erythroid/hematopoietic gene expression, loss of blood formation, and fetal demise. Orthogonal *ex vivo* analyses of primary erythroid progenitors selectively depleted of these two RNA-binding proteins revealed that they mediate a combination of overlapping and isoform-specific impacts on hematopoietic lineage transcriptome, impacting both mRNA representation and exon splicing. These data lead us to conclude that PCBP1 and PCBP2 mediate functions critical to differentiation of the erythroid lineage.

KEYWORDS murine erythropoiesis, posttranscriptional controls, PCBP1, PCBP2, RNA-binding proteins, conditional gene inactivation

RNA-binding proteins participate in a complex array of posttranscriptional controls essential to cell type specification and somatic development. The critical roles of such posttranscriptional controls are most clearly apparent in settings of global silencing of transcription. Posttranscriptional controls of terminal erythroid differentiation constitute one such highly informative experimental model (1–5).

The poly(C) binding proteins (PCBPs) comprise a widely expressed and multifunctional family of KH domain RNA-binding proteins associated with numerous erythroid and nonerythroid mRNAs (6, 7). Studies focused on globin gene expression in cell culture models have revealed that the PCBPs can integrate nuclear controls over splicing and 3′ processing with cytoplasmic controls over mRNA stabilization and translation (8, 9). These controls are mediated to a large extent via direct interactions of PCBPs with pyrimidine-pure cytosine-rich motifs located at critical sites within nuclear transcripts and cytoplasmic mRNAs (8–13). Transcriptome-wide analyses in a number of experimental settings have further revealed that PCBPs control the structures,

Citation Ji X, Jha A, Humenik J, Ghanem LR, Kromer A, Duncan-Lewis C, Traxler E, Weiss MJ, Barash Y, Liebhaber SA. 2021. RNA-binding proteins PCBP1 and PCBP2 are critical determinants of murine erythropoiesis. Mol Cell Biol 41:e00668-20. https://doi.org/10.1128/MCB.00668-20.

Address correspondence to Xinjun Ji, jixinjun@pennmedicine.upenn.edu.

Received 23 December 2020
Returned for modification 30 January 2021
Accepted 20 June 2021
Accepted manuscript posted online 28 June 2021
Published 24 August 2021

abundance, and functions of a wide array of mRNAs encoded by multiple gene subsets throughout the mammalian transcriptome (11, 12).

The PCBPs are encoded by genes representing four dispersed loci: *Pcbp1* to *Pcbp4*. The ubiquitous expression profiles of the major isoforms *Pcbp1* and *Pcbp2* contrast with the lower and more restricted expression of *Pcbp3* and *Pcbp4* (14–17). In contrast to the multiexonic gene of *Pcbp2*, *Pcbp1* is carried by an intronless gene that evolved by retrotransposition of a fully processed *Pcbp2* mRNA isoform (14, 16). The remarkably high level of structural conservation of the *Pcbp1* and *Pcbp2* homologs across eukaryotic taxa suggests strong evolutionary constraints in their functions (17).

The PCBP1 and PCBP2 proteins appear to have shared as well as isoform-specific functions (18–20). Recently we have shown that *Pcbp1* and *Pcbp2* constitute essential genes in mice (21); homozygous germ line inactivation of *Pcbp1* renders embryos nonviable in the peri-implantation stage (between E4.5 and E8.5), while *Pcbp2*-null mouse embryos undergo normal development through E12.5/13.5, at which point they undergo a loss in viability and develop a complex array of phenotypic defects. These defects prominently include alterations in the hematopoietic system (21). The very early (preimplantation) loss of *Pcbp1*-null embryos obviates detection of an *in vivo* impact of PCBP1 on hematopoiesis.

In the current study, we specifically focus on the impact of *Pcbp1* and *Pcbp2* on hematopoietic differentiation. The conditional, erythroid-specific inactivation of the *Pcbp1* and/or *Pcbp2* locus in the developing mouse embryo in conjunction with targeted *ex vivo* depletions of these proteins in primary hematopoietic cells reveals that the PCBPs play a critical role in mammalian erythropoiesis.

RESULTS

Selective loss of *Pcbp1* or *Pcbp2* in the erythroid lineage is compatible with embryonic viability and adult function. To explore the individual role(s) of *Pcbp1* and *Pcbp2* in mouse erythropoiesis, we selectively inactivated the corresponding genes in the erythroid lineage of the developing mouse embryo. Mice homozygous for a floxed *Pcbp2* allele (*Pcbp2*$^{fl/fl}$) were crossed with an *EpoR-cre* line. The *EpoR-cre* locus is composed of a Cre recombinase open reading frame (ORF) inserted within the endogenous erythropoietin receptor (*EpoR*) locus (22). EPOR is specifically activated at the erythroid burst-forming unit (BFU-E) stage erythroid differentiation and is maximally expressed in proerythroblasts within the erythroid CFU (CFU-E) (22, 23). *EpoR-cre-m*ediated recombination within the floxed *Pcbp2* locus deletes the first two exons of *Pcbp2*, thus inactivating gene expression in the erythroid lineage (21).

Cre-mediated inactivation of the PCBP2 locus was confirmed by DNA, RNA, and protein analyses of erythroid cells isolated from *Pcbp2*$^{fl/fl}$/*EpoR-Cre* fetal livers at E14.5 (Fig. 1A to C). *Pcbp2*$^{fl/fl}$/*EpoR-cre* embryos at E14.5 were developmentally intact (Fig. 1D), and corresponding adult mice appeared entirely normal, with the sole exception of a minor decrease in platelet levels (data not shown). Thus, in contrast to the embryonic lethality and hematopoietic abnormalities seen in germ line *Pcbp2*-null mice (21), the selective homozygous inactivation of the *Pcbp2* loci during erythroid lineage development failed to have an impact on hematopoiesis or overall development.

We next intercrossed *EpoR-cre* mice with mice carrying floxed *Pcbp1* loci. *Pcbp1* inactivation was confirmed by analyses of *Pcbp1*$^{fl/fl}$/*EpoR-cre* embryonic liver erythroid cells (Fig. 2A to C). *Pcbp1*$^{fl/fl}$/*EpoR-cre* mice were born at the expected Mendelian ratio, and the corresponding adults were within normal weight range compared to littermate controls. However, when assessed at E14.5, the *Pcbp1*$^{fl/fl}$/*EpoR-cre* embryos were observed to be pale compared to littermate controls (Fig. 2D). This pallor, along with alterations in a subset of red cell indices (RDW-CV and RDW-SD) and an elevated reticulocyte count suggested a mild level of erythroid stress in the *Pcbp1*$^{fl/fl}$/*EpoR-cre* adults (data not shown). Thus, the selective homozygous inactivation of *Pcbp1* loci by *EpoR-cre* resulted in nonlethal and compensated alterations in the hematopoietic pathway.

Combined inactivation of the *Pcbp1* and *Pcbp2* loci impacts erythroid lineage formation and embryonic viability. To further explore the *in vivo* functional relationships of the two *Pcbp* isoforms in the context of hematopoiesis, we generated intercrosses

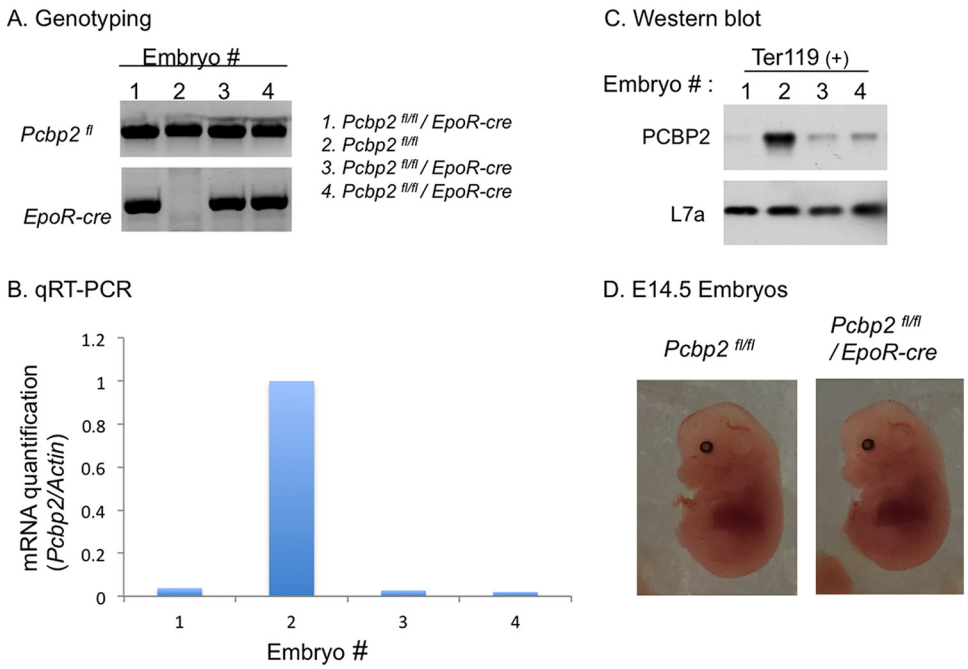

FIG 1 Embryos lacking *Pcbp2* in the erythroid lineage (*Pcbp2*$^{fl/fl}$/*EpoR-cre*) appear normal at E14.5. (A) Genotyping. E14.5 embryos generated from a cross between *Pcbp2*$^{fl/fl}$ and *Pcbp2*$^{fl/fl}$/*EpoR-cre* mice were genotyped with primers specific for the floxed *Pcbp2* and *EpoR-cre* loci. The genotypes of each of four embryos in a single litter are summarized to the right of the gel. (B) RNA analysis. The Ter119^{+}-enriched cells isolated from the livers of embryos (in panel A) were analyzed for *Pcbp2* mRNA. (C) Protein analysis. The Ter119^{+}-enriched cells (as in panel B) were assessed for PCBP2 protein content by Western analysis using a monospecific PCBP2 antibody (see Materials and Methods). Ribosomal protein L7a served as a loading control. (D) Embryo appearance. A *Pcbp2*$^{fl/fl}$/*EpoR-cre* E14.5 embryo (right) demonstrated normal appearance compared with a *Pcbp2*$^{fl/fl}$ littermate control (left).

of mice carrying the floxed *Pcbp1* and *Pcbp2* alleles and the *EpoR-cre* locus. Mice compound heterozygous for inactivation of the two *Pcbp* loci (*Pcbp1*$^{fl/wt}$/*Pcbp2*$^{fl/wt}$/*EpoR-cre*) were born at normal Mendelian ratios and appeared healthy at 2 months old, with normal complete blood counts (CBCs). The same intact functional state was observed for embryos that were *Pcbp2* null in the erythroblast lineage combined with *Pcbp1* haploidy (*Pcbp1*$^{fl/wt}$/*Pcbp2*$^{fl/fl}$/*EpoR-cre*) (Fig. 3A). In addition, mice with this genotype were viable at birth and as adults. In contrast, homozygosity for *Pcbp1* inactivation in combination with *Pcbp2* haploidy (*Pcbp1*$^{fl/fl}$/*Pcbp2*$^{fl/wt}$/*EpoR-cre*) was embryonic lethal. Analysis of E14.5 embryos with this genotype demonstrated marked overall pallor with faint and atrophic livers (Fig. 3B). In addition, mice with this genotype were embryonic lethal. These observations led us to conclude that there was a level of redundancy in *Pcbp1* and *Pcbp2* functions in the erythroid developmental pathway as well as a predominant role for PCBP1 versus PCBP2 in this process.

The most severe hematopoietic phenotype was observed for embryos compound homozygous for loss of the *Pcbp1* and *Pcbp2* loci (Fig. 3). These embryos (*Pcbp1*$^{fl/fl}$/*Pcbp2*$^{fl/fl}$/*EpoR-cre*) had markedly pale yolk sacs at E11.5 (Fig. 3C), extreme overall pallor and absence of liver erythropoiesis at E12.5 (Fig. 3D), and loss of viability by E13.5 (Fig. 3E). Thus, the complete loss of *Pcbp1* in the erythroid lineage is well tolerated when both *Pcbp2* loci are functioning, is embryonic lethal in the context of *Pcbp2* haploidy, and is even more devastating in terms of erythroid development and embryonic viability in embryos that are compound homozygous for inactivation of *Pcbp1* and *Pcbp2* (*Pcbp1*$^{fl/fl}$/*Pcbp2*$^{fl/fl}$/*EpoR-cre*). The foregoing observations support a dose dependency in the combined activities of *Pcbp1* and *Pcbp2* on erythropoiesis, with a predominant role played by *Pcbp1*.

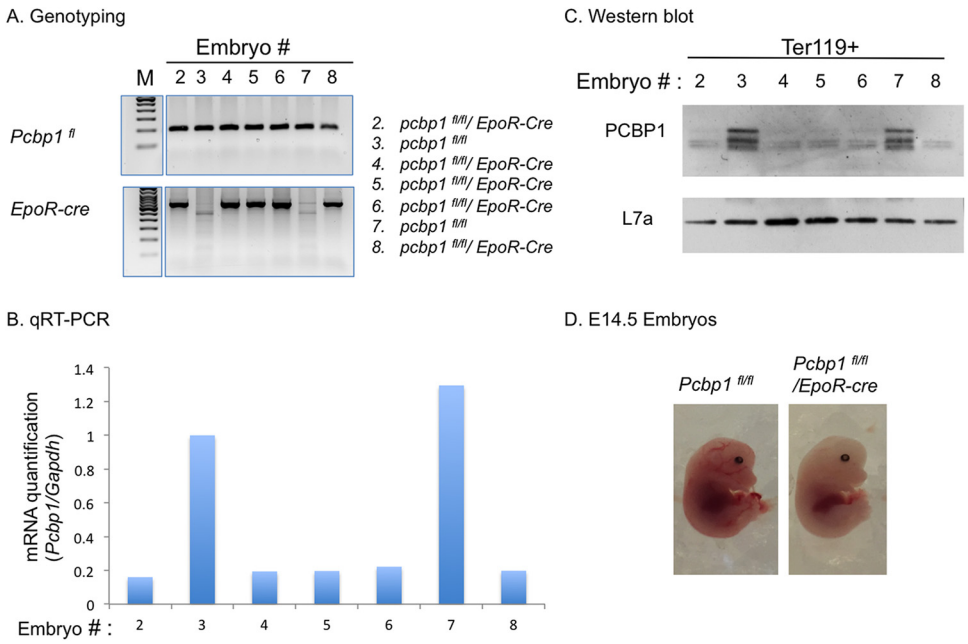

FIG 2 Embryos lacking *Pcbp1* in the erythroid lineage (*Pcbp1*$^{fl/fl}$/*EpoR-cre*) demonstrate mild pallor at E14.5. (A) Genotyping. E14.5 embryos generated from a cross between *Pcbp1*$^{fl/fl}$ and *Pcbp1*$^{fl/fl}$/*EpoR-cre* mice were genotyped by PCR for the floxed *Pcbp1* and *EpoR-cre* loci. The genotypes of seven embryos in a single litter are summarized to the right of the gel. (B) RNA analysis. Ter119^{+}-enriched cell populations from each of the indicated embryos (as in panel A) were analyzed for *Pcbp1* mRNA. (C) Protein analysis. The Ter119^{+}-enriched cell populations (as in panel B) were assessed by Western analysis with a monospecific PCBP1 antibody. Ribosomal protein L7a served as a loading control. (D) Embryo appearance. The *Pcbp1*$^{fl/fl}$/*EpoR-cre* E14.5 embryo (right) demonstrated mild pallor compared with a *Pcbp1*$^{fl/fl}$ littermate control (left).

Orthogonal evidence for a predominant role of PCBP1 in erythroid terminal differentiation. An orthogonal assessment of *Pcbp1* and *Pcbp2* functions in terminal erythroid differentiation was carried out in the mouse erythroleukemia (MEL) cell culture model (24). Depletion of *Pcbp2* by short hairpin RNA (shRNA) treatment had no appreciable impact on the induction of terminal erythroid differentiation, while a parallel depletion of *Pcbp1* from the MEL cells resulted in a dramatic blockade of hemoglobin synthesis (data not shown). These data further support a predominant role for *Pcbp1* compared to *Pcbp2* in murine erythroid differentiation.

Distinct contributions of *Pcbp1* and *Pcbp2* to the erythroid lineage as revealed by transcriptome analysis. While PCBP1 and PCBP2 protein structures are highly conserved and share a C-rich binding motif (14–17, 25), these two proteins have been shown to function both redundantly as well as with isoform specificity in various contexts (21, 26–33). A combination of redundant and isoform-specific functions in hematopoiesis would be consistent with the results of the preceding conditional gene inactivation studies (Fig. 1 and 3). To further explore the relative roles of PCBP1 and PCBP2 in hematopoiesis, we analyzed the impacts of selective depletion of each protein on the transcriptomes of primary hematopoietic progenitors induced to differentiate *ex vivo* under controlled conditions (34, 35). This *ex vivo* culture system supports terminal erythroblast proliferation and differentiation in a manner that closely mimics the *in vivo* terminal proliferation and maturation of erythroid cells (35). This experimental model, in which differentiation is monitored in a quantitative manner by flow cytometry, allows for erythroid cells at particular developmental stages to be identified and analyzed (35).

Sets of shRNAs targeting PCBP1, PCBP2, and nontargeting control sequences were used to assess the impact of PCBP depletion on *ex vivo* erythroid differentiation. Hematopoietic progenitor cells were affinity purified from wild-type E14.5 fetal livers, expanded, and selectively depleted of *Pcbp1* or *Pcbp2* using 4 distinct shRNAs for each

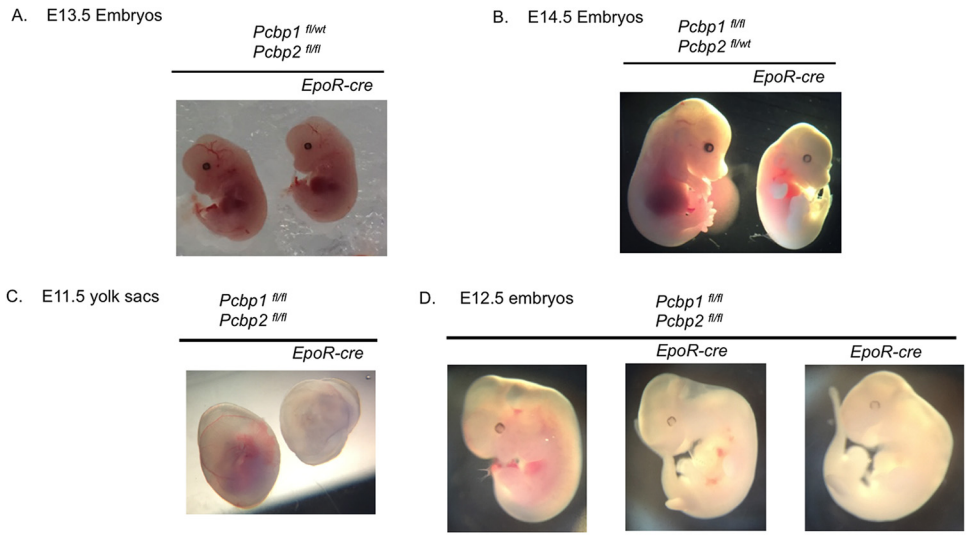

E. Adults

Genotype	*Pcbp1* $^{fl/wt}$ *Pcbp2* $^{fl/fl}$	*Pcbp1* $^{fl/fl}$ *Pcbp2* $^{fl/fl}$	*Pcbp1* $^{fl/wt}$ *Pcbp2* $^{fl/fl}$ *EpoR-cre*	*Pcbp1* $^{fl/fl}$ *Pcbp2* $^{fl/fl}$ *EpoR-cre*
Post Natal	10	18	14	0

FIG 3 Compound conditional inactivations of the *Pcbp1* and *Pcbp2* loci in the erythroid lineage reveal their essential roles in development of erythroid activity and in sustaining embryonic viability. (A) The mouse embryo with an erythroid lineage lacking PCBP2 combined with haploidy for PCBP1 appears normal at E13.5. A *Pcbp1*$^{fl/wt}$/*Pcbp2*$^{fl/fl}$/*EpoR-cre* E13.5 embryo is shown next to corresponding littermate control (floxed alleles without *EpoR-cre*). Embryos with the *Pcbp1*$^{fl/wt}$/*Pcbp2*$^{fl/fl}$/*EpoR-cre* genotype retain viability through term and into adult life. (B) The mouse embryo with an erythroid lineage lacking PCBP1 combined with haploidy for PCBP2 is small and pale at E14.5. A *Pcbp1*$^{fl/fl}$/*Pcbp2*$^{fl/wt}$/*EpoR-cre* embryo is shown next to the corresponding littermate control (floxed alleles without *EpoR-cre*). Embryos with the *Pcbp1*$^{fl/fl}$/*Pcbp2*$^{fl/wt}$/*EpoR-cre* genotype are embryonic lethal. (C) Combined homozygous inactivation of PCBP1 and PCBP2 loci results in marked loss of erythroid activity at E11.5. The yolk sacs of two E11.5 littermate embryos are shown along with their indicated genotypes. (D) E12.5 embryos with combined homozygous inactivation of the *Pcbp1* and *Pcbp2* loci are markedly pale. The embryos shown are from a single litter; corresponding genotypes are shown above each embryo. (E) Compound homozygous inactivation of *Pcbp1* and *Pcbp2* in the erythroid lineage is embryonic lethal. The numbers in the table reflect a total of 42 embryos from a total of 7 litters.

isoform. A set of nontargeting (control) shRNAs were used in parallel to control for nonspecific shRNA-induced perturbations of the transcriptome (34, 36).

RNA from each population was isolated at days 0 and 2 of induced differentiation. Sequencing of these RNA populations yielded approximately 35 million reads per sample. Analyses of the transcriptomes at day 0 confirmed an efficient depletion of PCBP1 or PCBP2 (>90%) for both PCBP1 and PCBP2 mRNAs (Fig. 4A) and proteins (Fig. 4B). The differential gene expression (DGE) analysis of the transcriptome sequencing (RNA-seq) data sets revealed that *Pcbp1* had a greater overall impact on gene expression than did *Pcbp2* (Fig. 5). This difference was observed both prior to and subsequent to erythroid induction (days 0 and 2, respectively) (see Table S2 in the supplemental material). It was additionally noted that the overall number of impacted genes was substantially greater at day 2 versus day 0, a trend that parallels the major shift in transcriptome composition during erythroid differentiation (37). Pathway analysis revealed significant enrichment for pathways relevant to chromatin assembly, cell adhesion, cell differentiation, regulation of signal transduction, cellular response to stress, cell proliferation, regulation of mitotic cell cycle, and erythroid differentiation after erythroid development induction (see Table S3 in the supplemental material).

The degree of overlap between the sets of *Pcbp1*- and *Pcbp2*-impacted genes was evaluated next. This overlap was minimal at day 0 but was substantially increased at day 2, in parallel with the overall increase in the number of impacted genes in the

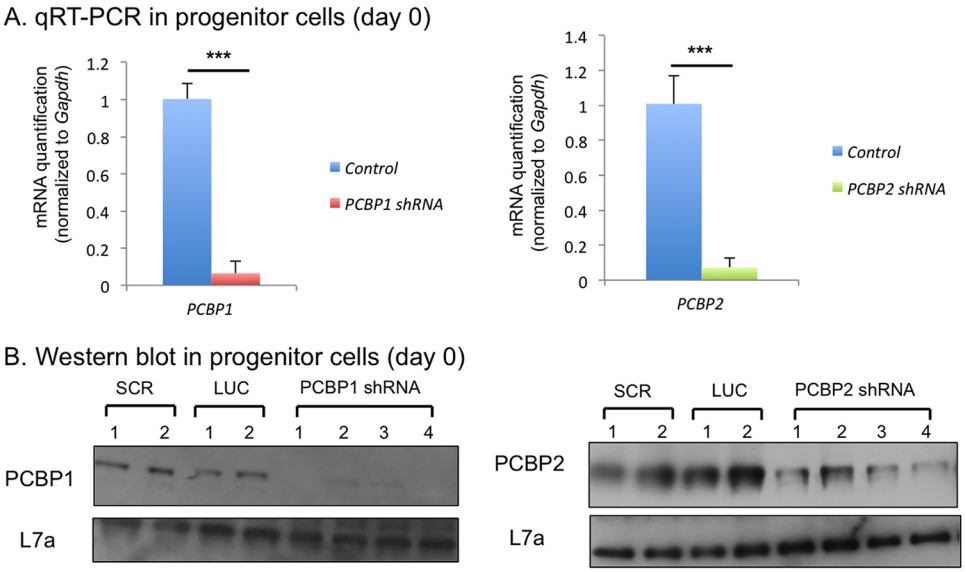

FIG 4 Selective depletion of PCBP1 and PCBP2 in hematopoietic stem cell (HSC)/progenitor cells. (A) Depletions of *Pcbp1* and *Pcbp2* mRNAs in primary HSC/progenitor cells. MSCV-PIG (puromycin-IRES-GFP)-based shRNAs targeting either PCBP1 or PCBP2 were transduced into HSC/progenitor cells purified from wild-type E14.5 mouse livers. The impact of the targeted depletions was quantified 2 days after transfection by qRT-PCR (with values normalized to corresponding glyceraldehyde-3-phosphate dehydrogenase [GAPDH] mRNA levels). *P* values were calculated by comparing the impact of *Pcbp2* and *Pcbp1* depletion with the result from parallel controls. ***, $P < 0.001$. (B) Western analysis. The protein analysis confirms efficient depletion of PCBP1 and PCBP2 proteins in shRNA-transduced cells. L7a, large ribosomal subunit 7a. The shRNAs are abbreviated as follows: Scr, Scrambled; Luc, luciferase.

differentiating erythroblasts (Fig. 5A and B). The differential impacts resulting from *Pcbp1* versus *Pcbp2* depletions during erythroid induction noted in this study were consistent with the distinct patterns and timing of embryonic lethality observed secondary to somatic loss of these two isoforms (21). Thus, these DGE studies supported a combination of redundancy and isoform specificity in *Pcbp* isoform activities in the differentiating erythroid lineage.

Impacts of *Pcbp1* and *Pcbp2* on mRNA expression appear to reflect both direct and indirect mechanisms. To explore the mechanisms of *Pcbp* impact on the erythroid transcriptome, we searched for C-rich binding site motifs in target mRNAs. This search focused on 3′ untranslated regions (UTRs) of mRNAs that were impacted by depletion of PCBP1 or PCBP2 during the process of the *ex vivo* erythropoietic differentiation process. Past studies have demonstrated that canonical C-rich binding sites in 3′ UTRs within target mRNAs are linked to major pathways of PCBP-mediated posttranscriptional control, including mRNA stability and 3′ processing (8, 11, 12). The current analysis revealed a significant enrichment in cognate *Pcbp1* and *Pcbp2* binding sites (CISBP-RNA database [38]) in 3′ UTRs of genes downregulated in the differentiating hematopoietic precursors upon depletion of *Pcbp1* (Fig. 5C, top) or *Pcbp2* (Fig. 5C, bottom). Pathway analysis of these genes revealed significant enrichment for pathways relevant to chromatin assembly, nucleosome organization, RNA metabolism, chromatin silencing, and negative regulation of gene expression (see Table S4 in the supplemental material). This finding supports a model in which direct PCBP binding plays a positive role in the expression of a subset of mRNAs during the differentiation process.

Remarkably, the motif searches revealed additional motifs, distinct from the poly(C)-rich sequences, that were also enriched in 3′ UTRs of PCBP-impacted mRNAs. Of particular interest was the identification of the consensus motif for RBM38 (GU rich) for many genes (Fig. 5D; see Table S5 in the supplemental material). RBM38 is of particular interest as this RNA-binding protein is downregulated when either *Pcbp1* or *Pcbp2* was depleted (data not shown), likely due to the presence of several C-rich motifs in its 3′ UTR, and has been reported to have a critical role in erythroid differentiation (39–42). These data indicated

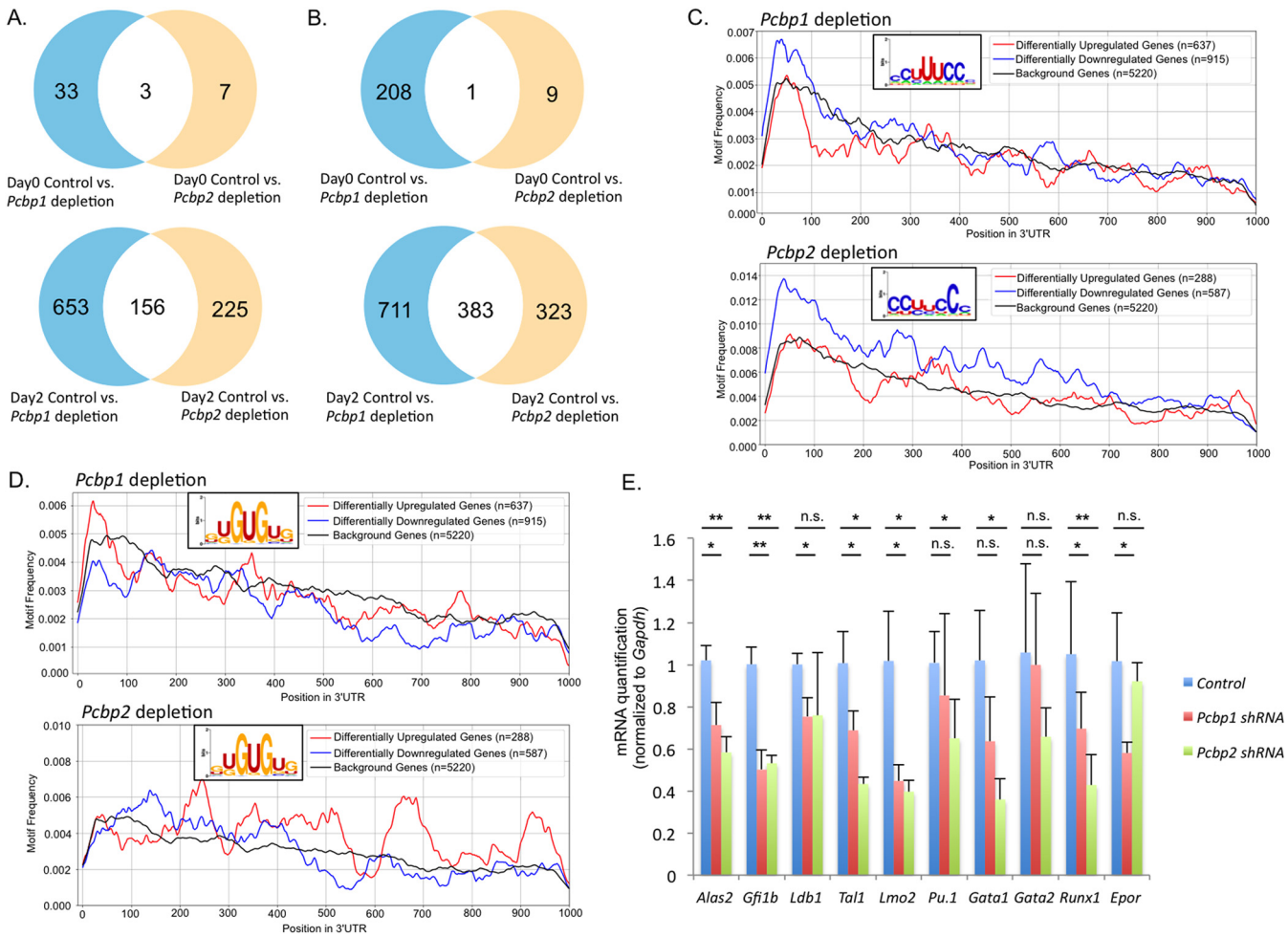

FIG 5 Comparative impacts of *Pcbp1* and *Pcbp2* depletions on hematopoietic transcriptomes during *ex vivo* erythroid differentiation. (A) Genes upregulated by *Pcbp1* or *Pcbp2* depletions. (Top) Venn diagram displays the numbers of genes in primary hematopoietic progenitors that are upregulated upon *Pcbp1* or *Pcbp2* depletion prior to erythroid induction (day 0). *Pcbp1* depletion versus control is in light blue, *Pcbp2* depletion versus control is in light brown, and genes upregulated by both *Pcbp1* and *Pcbp2* depletions are in white (overlap). (Bottom) A Venn diagram displays the numbers of genes upregulated by depletion of *Pcbp1* or *Pcbp2* after 2 days of induced erythroid differentiation (day 2). The color code is as in the top diagrams. (B) Genes downregulated by *Pcbp1* or *Pcbp2* depletions. (Top) A Venn diagram displays the numbers of genes in primary hematopoietic progenitors that are downregulated upon *Pcbp1* or *Pcbp2* depletion prior to erythroid induction (day 0). The color code is as in panel A. (Bottom) A Venn diagram displays the numbers of genes that are downregulated by depletion of *Pcbp1* or *Pcbp2* after 2 days of induced erythroid differentiation (day 2). The color code is as in panel A. (C) Pyrimidine-pure/C-rich motifs are enriched in the 3′ UTRs of genes downregulated upon *Pcbp1* and *Pcbp2* depletions. (Top) Motif maps showing the frequency and positioning of *Pcbp1* motifs (defined in the CISBP-RNA database [38]) in the 3′ UTRs of genes that are impacted (upregulated in red and downregulated in blue) upon *Pcbp1* depletion in primary embryonic erythroid cells (combined day 0 and day 2 data). The *Pcbp1* motifs are significantly enriched in the downregulated genes relative to the control as background (FDR corrected $P = 3.56e{-}06$, one-sided Fisher's exact test). Motif significance was computed with sequences up to 1,000 nucleotides (nt) into the 3′ UTRs of these genes. Frequencies were smoothed using a running mean of 50 nt. (Bottom) Motif maps showing the frequency and positioning of *Pcbp2* motifs (CISBP-RNA database [38]) in the 3′ UTRs of genes that are upregulated (red) and downregulated (blue) upon *Pcbp2* depletion in primary embryonic erythroid cells (combined day 0 and day 2 data). The color code is as in the top panel. The *Pcbp2* motifs are significantly enriched in the downregulated genes, with the control as the background (FDR corrected $P = 2.09e{-}15$, one-sided Fisher's exact test). Motif significance was computed with sequences up to 1,000 nt into the 3′ UTRs of these genes. Frequencies were smoothed using a running mean of 50 nt. (D) The *Rbm38* motif (GU-rich) is significantly enriched in the 3′ UTRs of mRNAs that are upregulated upon *Pcbp2* depletion. (Top) Motif maps showing the frequency and positioning of *Rbm38* motifs in the 3′ UTRs of genes that are upregulated (red) and downregulated (blue) upon *Pcbp1* depletion (combined day 0 and day 2 data). The *Pcbp1* motif is not significantly enriched in either upregulated genes or downregulated genes relative to control depletion as the background (black). Motif significance was computed with sequences up to 1,000 nt into the 3′ UTRs of these genes. Frequencies were smoothed using a running mean of 50 nt. (Bottom) Motif maps showing the frequency and positioning of the *Rbm38* motif in the 3′ UTRs of genes that are upregulated (red) and downregulated (blue) upon *Pcbp2* depletion (combined day 0 and day 2 data). The *Rbm38* motif is significantly enriched in the genes upregulated upon Pcbp2 depletion, with control depletion as the background (FDR corrected $P = 0.003$, one-sided Fisher's exact test). Motif significance was computed with sequences up to 1,000 nt into the 3′ UTRs of these genes. Frequencies were smoothed using a running mean of 50 nt. (E) Impact of *Pcbp1* and *Pcbp2* depletions on genes linked to hematopoietic/erythropoietic differentiation and function. RT-PCR analyses were carried out on RNA isolated from HSC/progenitor cells post-erythroid induction (day 2 cells). The graph reflects the average and standard deviation of results from 10 separate RNA samples. The shRNAs targeting *Pcbp1* are shown as 1-1, 1-3, and 1-4, the shRNAs targeting *Pcbp2* are shown as 2-1, 2-2, 2-3, and 2-4, and the control shRNAs are shown as *scr1*, *scr2*, *Luc1*, and *Luc2*. Each mRNA value was normalized to the corresponding *Gapdh* mRNA level prior to calculation of the averages and significance values. *P* values were calculated by comparing the impact of *Pcbp1* (top row) and *Pcbp2* (low row) depletion with values from parallel controls. *, $P < 0.05$; **, $P < 0.01$; n.s., not significant.

that the *Rbm38* motif was not significantly enriched in the 3′ UTRs of genes impacted by *Pcbp1* depletion. On the other hand, the *Rbm38* motif was enriched in the 3′ UTRs of upregulated genes after *Pcbp2* was depleted from the primary cells (Fig. 5D). Pathway analysis of these genes containing RBM38 binding sites in the encoded 3′ UTRs revealed significant enrichment for pathways relevant to cell death, organ development, and cell signaling (Table S5). In sum, these data support roles for PCBPs in modulating the developing erythroid transcriptome via direct recognition of the cognate poly(C)-rich motif as well as via indirect actions mediated by alterations in expression of downstream RNA-binding proteins such as RBM38.

Targeted analyses confirm redundant and unique impacts of *Pcbp1* and *Pcbp2* on erythroid lineage transcripts. The global transcriptome analyses of primary hematopoietic cells depleted of *Pcbp1* and *Pcbp2* (described above) pointed to a combination of redundant and isoform-specific actions of the PCBPs on erythroblast gene expression (described above). To further explore this combination of mechanisms, we carried out targeted analyses of 10 genes whose encoded proteins have well-documented roles in hematopoietic lineage commitment and/or erythroid differentiation (Fig. 5E). These data revealed *Pcbp1* specifically impacts 2 genes (*Ldb1* and *EpoR*), *Pcbp2* specifically impacts 2 genes (*Pu.1* and *Gata1*), and the impacts of *Pcbp1* and *Pcbp2* depletions on the remaining 6 genes (*Alas2*, *Gfi1b*, *Tal1*, *Lmo2*, *Runx1*, and *Gata2*) overlap. These data support the conclusion that the two *Pcbp* isoforms mediate redundant as well as isoform-specific roles on erythroid lineage development.

***Pcbp1* and *Pcbp2* demonstrate different impacts on exon splicing in the erythroid transcriptome.** *Pcbp*s have well-described impacts on alternative splicing pathways in multiple settings (9, 11, 26, 43, 44). With this in mind, we next analyzed our RNA-seq data for cassette exon inclusion/exclusion rates in the setting of *Pcbp1* and *Pcbp2* depletion in the primary hematopoietic cell culture model (Fig. 6A and B). This alternative splicing (AS) analysis revealed a greater impact by *Pcbp1* compared to *Pcbp2* depletions at both days 0 and 2 of erythroid induction (see Table S6 in the supplemental material). This difference was observed for enhanced as well as repressed cassette exons. Pathway analysis of these genes with AS revealed significant enrichment for pathways relevant to RNA processing, RNA splicing, erythrocyte homeostasis, and erythrocyte differentiation (see Table S7 in the supplemental material). Thus, the AS and DGE analyses were consistent in revealing that a large subset of the impacts of the two *Pcbp* isoforms on the transcriptome were isoform specific, that the impact of *Pcbp1* had a greater impact than *Pcbp2*, and that the number of events impacted by *Pcbp* depletions increased during erythroid lineage induction.

We next searched for evidence of direct impacts of PCBPs on splicing in the erythroid transcriptome. MEME analysis of mRNAs whose alternative exon splicing was impacted by *Pcbp1* and *Pcbp2* depletion revealed enrichment for C-rich motifs in the splice-proximal regions of the alternatively spliced exons (Fig. 6C). In the setting of both *Pcbp1* and *Pcbp2* depletions, a C-rich motif is significantly enriched in the region of the splice acceptor site of repressed cassette exons; *Pcbp1* depletion was linked to significantly enriched peaks in the cassette exons with repressed inclusion (Fig. 6C, blue) adjacent to the splice acceptor sites (nucleotides [nt] −300 to +50; false-discovery rate [FDR] corrected $P = 3.23e-06$) and splice donor sites (nt −50 to +300; FDR corrected $P = 0.01$). Enriched peaks in the cassette exons with enhanced inclusion (Fig. 6C, red) in the intronic region were also visually apparent in proximity to the splice donor site (nt +150 to +300), although this did not reach statistical significance (P = not significant [NS]).

Upon *Pcbp2* depletion, there were visually apparent peaks of enrichment of the C-rich motif in the cassette exons with repressed inclusion (Fig. 6C, blue) in the intronic region in proximity to the splice donor site (nt +100 to +175 and +250 to +300) and in the intronic region in proximity to the splice acceptor site (nt −50 to 0). There were also visually apparent enriched peaks in the cassette exons with enhanced inclusion (Fig. 6C, red) in the intronic region near the splice acceptor site (nt −300 to −225, −150 to −100, and −50 to 0). These enrichments of C-rich motifs associated with

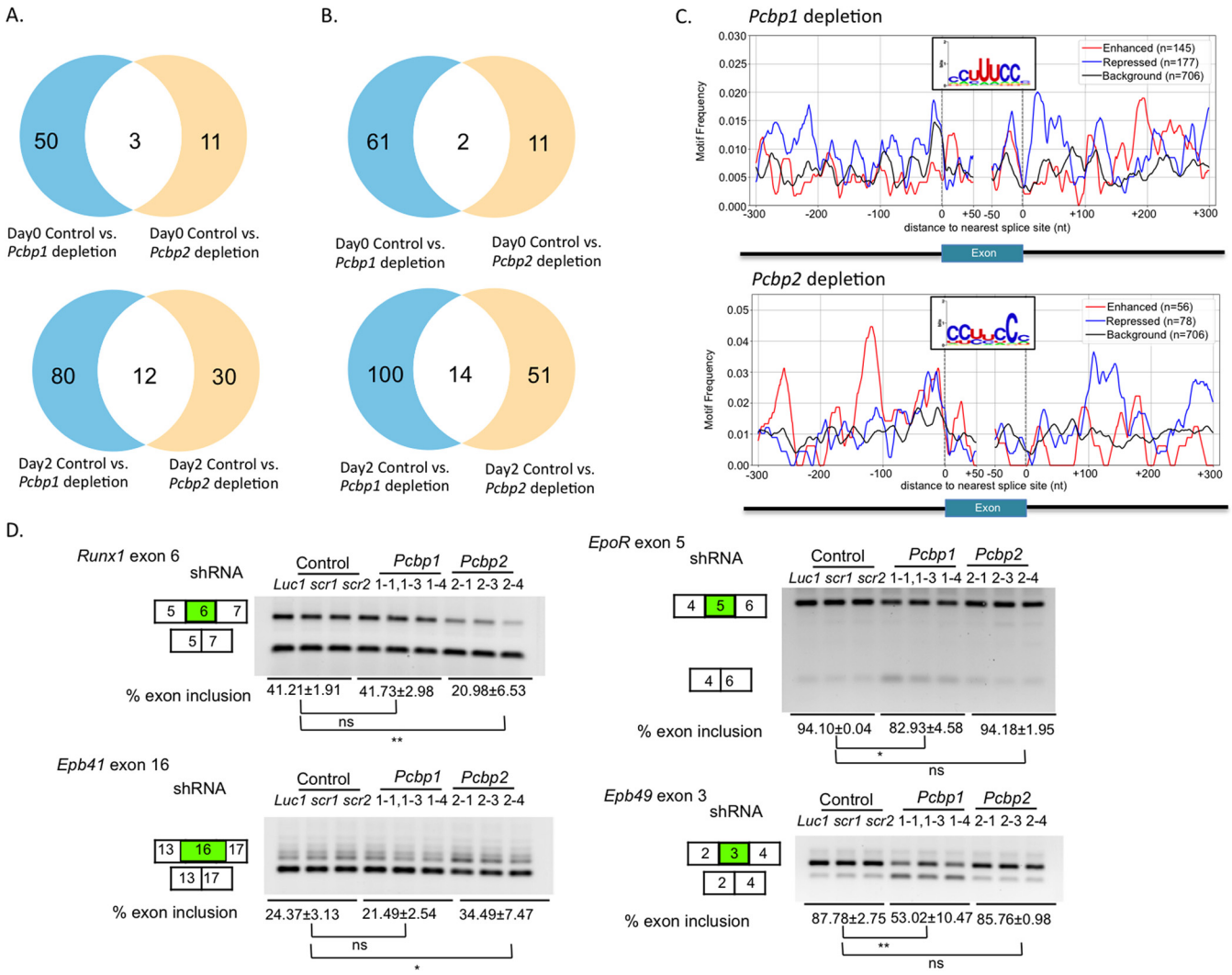

FIG 6 *Pcbp1* and *Pcbp2* have distinct impacts on alternative exon splicing in primary hematopoietic cells. (A) Enhanced exon inclusion events in cells depleted of *Pcbp1* or *Pcbp2* cells at days 0 and 2 of erythroid induction highlight isoform-specific functions. (Top) A Venn diagram displays the numbers of exons whose inclusion is enhanced subsequent to *Pcbp1* (blue) and *Pcbp2* (yellow) depletion prior to induction (day 0). Each binary comparison is noted below the corresponding circle. Exons whose splicing is impacted by both *Pcbp1* and *Pcbp2* depletions are shown in the overlap (white). (Bottom) A Venn diagram displays the numbers of exons whose inclusion is enhanced subsequent to *Pcbp1* (blue) and *Pcbp2* (yellow) depletion after 2 days of erythroid induction (day 2). Each binary comparison is noted below the corresponding circle. Exons whose splicing is impacted by both *Pcbp1* and *Pcbp2* depletions are shown in the overlap (white). (B) Repressed exon inclusion in cells depleted of *Pcbp1* or *Pcbp2* at days 0 and 2 of erythroid induction. (Top) A Venn diagram displays the numbers of exons whose inclusion is repressed subsequent to *Pcbp1* (blue) and *Pcbp2* (yellow) depletion prior to induction (day 0). Each binary comparison is noted below the corresponding circle. Exons whose splicing is impacted by both *Pcbp1* and *Pcbp2* depletions are shown in the overlap (white). (Bottom) A Venn diagram displays the numbers of exons whose inclusion is repressed subsequent to *Pcbp1* (blue) and *Pcbp2* (yellow) depletion after 2 days of erythroid induction (day 2). Each binary comparison is noted below the corresponding circle. Exons whose splicing is impacted by both *Pcbp1* and *Pcbp2* depletions are shown in the overlap (white). (C) Distribution of consensus binding sites for *Pcbp1* and *Pcbp2* in proximity to alternatively spliced exons impacted by *Pcbp1* and *Pcbp2* depletion. (Top) Frequency and positions of *Pcbp1* motifs (CISBP-RNA database [38]) around the 3′ and 5′ splice sites of cassette exons whose inclusion is enhanced (red) and repressed (blue) by *Pcbp1* depletion on days 0 and 2 of erythroid inductions. Frequencies were smoothed using a running mean of 20 nucleotides (nt). The *Pcbp1* motif is significantly enriched in the cassette exons with repressed inclusion (blue) in the region of the splice acceptor site (nt −300 to +50; FDR corrected $P = 3.23e{-}06$) and the splice donor site (nt −50 to +300; FDR corrected $P = 0.01$). *P* values were computed using one-sided Fisher's exact test. (Bottom) Frequency and positions of *Pcbp2* motifs (CISBP-RNA database [38]) in proximity to cassette exons that are enhanced (red) and repressed (blue) upon *Pcbp2* depletion at days 0 and 2 of induced erythroid differentiation. Frequencies were smoothed using a running mean of 20 nt. The apparent enrichment of C-rich motifs near the splice acceptor site of repressed exons could not be firmly established as statistically significant due to low number of events in the enhanced set. (D) RT-PCR validation of alternative splicing events. RT-PCR was performed on day 2 RNAs for alternatively spliced exons in 4 genes that have clearly defined roles in hematopoietic lineage commitment: *Runx1*, exon 6; *EpoR*, exon 5; Epb41, exon 16; *Epb49*, exon 3. RNAs were purified from the E14.5 mouse liver and treated with the indicated shRNAs. Control shRNAs are shown as *luc1*, *scr1*, and *scr2*, *Pcbp1* shRNAs are shown as 1-1, 1-3, and 1-4, and *Pcbp2* shRNAs are shown as 2-1, 2-3, and 2-4. Alternatively spliced exons are indicated by green boxes. The percentage of exon inclusion is calculated and shown at the bottom of the gel (average ± standard deviation). *P* values were calculated by comparing the impact of *Pcbp2* and *Pcbp1* depletion with values from parallel controls. *, $P < 0.05$; **, $P < 0.01$, n.s., not significant.

Pcbp2 depletion could not be established as statistically significant due to low number of events in the enhanced and repressed set.

Analysis of genes with *Pcbp2*-impacted cassette exon splicing revealed significant enrichment for pathways relevant to hematopoietic development, mRNA processing, cellular localization, eryhthrocyte homeostasis, and erythroid differentiation (see Table S8 in the supplemental material).

Targeted validations of alternative exon splicing were carried out on transcripts selectively sensitive to either *Pcbp1* or *Pcbp2*. *Runx1* is a critical transcription factor for blood development (45–48). The data confirmed our previous finding that AS control of exon 6 splicing is specific to *Pcbp2* (26), and not responsive to depletion of *Pcbp1* (Fig. 6D, *Runx1*). Erythropoietin receptor (EPOR) is critical for terminal erythropoiesis (23). We confirmed that *Pcbp1*, but not *Pcbp2*, specifically impacts alternative splicing of exon 5 of the *EpoR* gene. This event is of functional significance as loss of exon 5 is predicted to trigger an NMD response, which would be consistent with the observed downregulation of *EpoR* mRNA by *Pcbp1* depletion (Fig. 5E). EPB41 and EPB49 are two red blood cell membrane proteins that are important/essential for terminal erythroid development (49–51). We found that *Pcbp2* specifically represses inclusion of exon 16 (knockdown of *Pcbp2* increases the inclusion of exon 16) of *Epb41* (Fig. 6D, *Epb41*), an exon shown by others to be important in late stage of erythropoiesis (49, 52–55). For *Epb49*, the data revealed that *Pcbp1* enhances splicing of exon 3, while *Pcbp2* lacks an effect (Fig. 6D, *Epb49*). These studies further substantiate the conclusion that the PCBP1 and PCBP2 isoforms have specific impacts on gene expression that are of direct relevance to erythroid development and function.

DISCUSSION

We have previously demonstrated that the paralogous RNA-binding proteins, PCBP1 and PCBP2, are independently essential for mouse embryonic viability (21). Here, we explore their tissue-specific requirement in erythroid lineage. The *EpoR-cre* driver used in these studies selectively inactivates floxed loci in the erythroid lineage beginning at E12.5 (22). Conditional knockouts revealed that individual loss of *Pcbp1* or *Pcbp2* failed to significantly impact the developing erythroid lineage (Fig. 1 and 2), while their combined loss resulted in a substantial loss of hematopoiesis: homozygous loss of *Pcbp1* in conjunction with haploidy for *Pcbp2* inactivation repressed erythroid development and resulted in embryonic lethality at E14.5, and compound homozygous inactivation of *Pcbp1* and *Pcbp2* loci resulted in an even more severe phenotype, with dramatic loss of fetal liver erythropoiesis and embryonic demise prior to E13.5 (Fig. 3). These findings led us to conclude that formation of the erythroid lineage and embryonic development can be supported individually by either *Pcbp1* or *Pcbp2*, while the combined loss of these two paralogs is incompatible with these critical processes.

Assessing the impact of individual depletions of *Pcbp1* and *Pcbp2* on the transcriptomes of primary hematopoietic progenitor cells induced toward erythroid differentiation revealed that subsets of genes were uniquely impacted by one or the other of the *Pcbp* isoforms, while others constitute an overlapping gene set (Fig. 5A and B). A similar combination of isoform-specific and shared (overlapping) impacts was observed in the analysis of alternative exon splicing (Fig. 6A and B). Thus, the transcriptome analyses of primary hematopoietic cells demonstrated a complex set of impacts of *Pcbp1* and *Pcbp2* on mRNA representation (DGE analysis) and structure (AS analysis), reflecting both isoform-specific and redundant impacts.

The motif analyses of our RNA seq data sets in primary hematopoietic precursors depleted of the individual *Pcbp* isoforms revealed significant enrichment of C-rich *Pcbp* binding sites within 3′ UTR sequences of genes that were downregulated upon *Pcbp1* or *Pcbp2* depletion (Fig. 5C). These data point to a direct positive role in enhancing the expression of a defined gene subset. The motif analysis of mRNAs whose exon splicing reactions were impacted by *Pcbp* depletion also had significant enrichment for C-rich motifs in proximity to the alternatively splice exons (Fig. 6C). This result is consistent

with our prior transcriptome-wide analysis of *Pcbp*-controlled exon splicing in a human hematopoietic cell line (K562 cells) which identified a significant enrichment of C-rich motifs adjacent to splice sites controlled by PCBPs (11). In the current study, this impact on exonic splicing is most prominently seen in the context of depletion of *Pcbp1* compared to *Pcbp2* (Fig. 6C). Targeted analysis of exon splicing further linked the roles of *Pcbp1*- and *Pcbp2*-mediated AS controls to erythroid development and highlighted isoform-specific functions (Fig. 6D).

While the foregoing studies supported a role for direct *Pcbp*-mRNA interactions in erythroid development, the fact that these linkages were only defined in a subset of the impacted genes suggested that additional RNAs may be regulated by *Pcbp*-dependent indirect pathways. Of particular interest was the observation that depletion of *Pcbp1* or *Pcbp2* caused a significant decrease in the expression of RBM38. This RNA-binding protein has been shown by others to be involved in posttranscriptional controls linked to erythroid differentiation (39–41). The impact of *Pcbp* depletion on *Rbm38* gene expression suggested that one or more of the actions of *Pcbp* genes may be indirect and mediated via RBM38 actions.

A final observation from the transcriptome analyses that merits mention is that the number of genes impacted by *Pcbp1* and *Pcbp2* depletions increased markedly subsequent to the 2 days of EPO-induced erythroid differentiation (Fig. 5B). These results suggest that some genes critical/important to erythroid differentiation may not be affected by *Pcbp1/2* prior to differentiation (day 0), but rather are affected during the differentiation process. The impact on the alternative exon splicing of the *Epb41* gene transcript is a good example of such differentiation-linked posttranscriptional regulation (Fig. 6D).

In summary, we demonstrate in the current report, using both *in vivo* and *ex vivo* models, that PCBPs work cooperatively to support pathways of gene expression that are essential to mouse erythroid development.

MATERIALS AND METHODS

Animals. All experiments were conducted in accordance with protocols approved by the Institutional Animal Care and Use Committee at the Perelman School of Medicine (University of Pennsylvania).

The floxed *Pcbp2* mouse line has been previously described (21), and the *EpoR*-cre line was a kind gift from Ursula Klingmüller (22).

Generation of mouse line carrying a floxed *Pcbp1* allele. CRISPR-Cas9-mediated gene editing (56) was utilized to flank the entire intronless *Pcbp1* locus with LoxP sites. Single-guide RNAs (sgRNAs) targeting the 5′ and 3′ flanking regions of *Pcbp1* (sequences available on request) were selected based on principles that minimize off-target effects (57). sgRNAs and tracrRNA (Alt-R CRISPR-Cas9 tracrRNA no. 1072532) were obtained from Integrated DNA Technologies (CA). The capped and polyadenylated Cas9 mRNA (L-7206; TriLink BioTechnologies) and the homology-directed repair (HDR) templates were microinjected into the cytoplasm of single-cell C57BL/6J embryos (Jackson Laboratory, no. 000664) at the Transgenic Mouse Facility of the University of Pennsylvania. The resultant pups were screened for LoxP sequence insertion by PCR (primer sequences available upon request) and confirmed by Sanger sequencing.

Conditional inactivation of *Pcbp1* and/or *Pcbp2* in the erythroid lineage. *Pcbp1* and *Pcbp2* loci were inactivated in the erythroid lineage by crossing the corresponding floxed *Pcbp1* or *Pcbp2* mouse lines with the *EpoR-cre* line (22). Offspring carrying the floxed *Pcbp* and *EpoR-cre* alleles were identified by PCR (21, 22).

***In vitro* expansion and differentiation of murine erythroblasts selectively depleted of *Pcbp1* and *Pcbp2*.** E14.5 fetal liver cell suspension was enriched for hematopoietic progenitors using the EasySep Hematopoietic Progenitor Cell Enrichment kit (StemCell Technologies, no. 19756) supplemented with biotin-conjugated CD71 antibody (BioLegend) (34, 36). The purified hematopoietic progenitor cells were cultured in expansion medium consisting of StemPro34 medium (Invitrogen) supplemented with 2 mM L-glutamine, 1% penicillin-streptomycin, 10 μM 1-thioglycerol, 1 μM dexamethasone, 0.5 U/ml erythropoietin, and 1% murine stem cell factor (SCF) (34) and infected immediately with MSCV-PIG (murine stem cell virus-puromycin-internal ribosome entry site [IRES]-green fluorescent protein [GFP])-based retroviruses encoding shRNAs that target *Pcbp1* and *Pcbp2*, as well as two sets of control shRNAs: luciferase and scrambled sequence (Table 1). The transduced cells were grown in expansion medium for 48 h. These cells were collected (day 0 cells) or washed and resuspended in differentiation medium (Iscove's modified Dulbecco's medium [IMDM] with 10% fetal calf serum [FCS], 10% potassium dodecyl sulfate [PDS], 2 mM L-glutamine, 10 μM 1-thioglycerol, 1% penicillin-streptomycin, 5% PFHM-II medium, and 5 U/ml erythropoietin [Amgen]) (34) and incubated for an additional 2 days (day 2 cells).

TABLE 1 Primer and shRNA sequences

Gene or shRNA	Primer sequence or shRNA designation[a]
Genes	
qRT-PCR	
Tal1	F: TTAGCCAGCCGCTCGCCTCA
	R: TGGTGAAGATGCGCCGCACT
Lmo2	F: GAAAGGAAGAGCCTGGACCC
	R: CACCACATGTCAGCAGGGAT
Ldb1	F: TGCTGAAGTGCCACGTCTTT
	R: CACGCTACTTCCGAAGCATTT
Gfi1b	F: CAGGGACAGTGTGGAGGTTC
	R: CTAGAAAGGACCGTGGCATT
Pu.1	F: GCTTCCCTTATCAAACCTTGTCCC
	R: CAGGCGAATCTTTTTCTTGCTGC
Alas2	F: ATTTGGGCATAAGCAGACAC
	R: CAGCTCCATGATTCTTCAGG
Beta actin	F: AAGGAGATTACTGCTCTGGCTCCTA
	R: ACTCATCGTACTCCTGCTTGCTGAT
Runx1	F: TCAGAAGTGTAAGCCCAGCA
	R: CTTTCGAAAACGCACCTCTC
Pcbp1	F: AATCAATGCCAGGCTTTCCTC
	R: TTAAAACCTGGAATTACCGACCAG
Pcbp2	F: CATGGGGAGCAGCTAGAACAGA
	R: TTAAAACCTGGAATCGCTGACTG
Gata1	F: GCCCAAGAAGCGAATGATTG
	R: GTGGTCGTTTGACAGTTAGTGCAT
Gata2	F: CACCCCTAAGCAGAGAAGCAA
	R: TGGCACCACAGTTGACACACT
Gapdh	F: TGTCAAGCTCATTTCCTGGTATGA
	R: TCTTACTCCTTGGAGGCCATGT
Epor	F: AGGTCCTGGAAGGCCGCACT
	R: AGGGTCCAGGTCGCTAGCGG
Alternative splicing RT-PCR	
mEpoR	F: CCTATGACCACCCACATCCG
	R: GCGTCAAGATGAGAGGGTCC
mDmtn	F: GGATGAGGACACCACAGAGC
	R: GATGGCAGCCAGATCCTTGT
mEpb41	F: AGCCATTGCTCAGAGTCAGGTCACAG
	R: CAGTTCACTGATGCTGGCATGGTGC
mRunx1	F: AATCCGCCACAAGTTGCCA
	R: ATGGATCCCAGGTACTGGTAGG
shRNAs	
Pcbp1 and *Pcbp2* shRNAs for fetal liver cells[b]	
shPcbp1-1	CTCCGCTAAGAATTTAAAGAAA
shPcbp1-2	GCACCGAGTGTGTGAAGCAGAT
shPcbp1-3	TGCCTACCAATGCCATCTTTAA
shPcbp1-4	CATGTAAGAGTGGAATGTTAAT
shPcbp2-1	CAAGGAGAATCTGTTAAGAAGA
shPcbp2-2	AACCGGATTCAGTGGCATTGAA
shPcbp2-3	CCCGACTAATGCCATCTTCAAA
shPcbp2-4	TCTGCACCAGTTGGCAATGCAA
shLuciferase	RHS1705
shScramble	RHS4346
Pcbp1 and *Pcbp2* shRNAs for MEL cells[c]	
shPcbp1	CGGCGTGCCGCAGTCCGTCACCGAGTGTG
shPcbp2	GGCCTATACCATTCAAGGACAGTATGCCA
shScramble	TR30013

[a]F, forward; R, reverse.
[b]The sequences shown are on the MSCV-PIG vector (Open Biosystems).
[c]The sequences shown are on the pGFP-V-RS or p-RFP-V-RS vector (Origene).

Transcriptome analysis (RNA-seq). One microgram of total RNA isolated at day 0 and day 2 cells from each *Pcbp1*- or *Pcbp2*-depleted sample (all RNA integrity number [RIN] values of >8.6) was used for library construction after poly(A) selection (Next Generation Sequencing Core, University of Pennsylvania). A total of 9 samples were generated from each of the two time points: three controls, *Pcbp1* knockdowns with three distinctly targeting shRNAs (shPcbp1-1, -3, and -4), and *Pcbp2* knockdowns with three distinctly targeting shRNAs (shPcbp2-1, -3, and -4). Sequencing was carried out using a 150-nt paired-end sequencing protocol. RNA-seq reads were aligned to GRCm38.p6 annotation using STAR after a quality check and trimming with FastQC and Trim Galore, respectively. Aligned bam files were sorted and indexed with Samtools.

Gene expression analysis. Transcriptome indices were prepared for Salmon (https://salmon.readthedocs.io/en/latest/salmon.html) with the GRCm38 mouse annotation. Transcripts per million RNA molecules (TPMs), length-scaled TPMs, and effective length quantifications were generated using as input trimmed RNA-seq reads and the Salmon transcriptome indices. Transcript-level TPMs were collapsed into gene-level TPMs with the Bioconductor package tximport. Reads mapping to rRNA, tRNA, and mitochondrial DNA were removed. EdgeR was used to compute $\log_2$ fold change and statistical significance of differential expression. Genes with a |fold change| of >1.5 and false-discovery rate of <0.1 were considered differentially expressed.

Alternative splicing analysis. Splicing events were quantified with MAJIQ and VOILA (58). Differential splicing was computed with the DeltaPSI module of MAJIQ. DeltaPSI quantifies differential splicing (inclusion or exclusion) of a junction between two conditions (e.g., control replicates versus *Pcbp1* or *Pcbp2* depletion replicates). Cassette splicing events with a |DeltaPSI| value of >0.10 were considered differentially spliced.

Motif enrichment analysis. One thousand nucleotides in the 3′ UTR sequences were extracted from differentially upregulated, downregulated, and background (nonregulated) genes and were searched by MEME (59) for enriched motifs as defined in the CISBP-RNA database (38). Motif maps of *Pcbp1*, *Pcbp2*, and *Rbm38* were constructed from the calculated frequencies of occurrence of corresponding motifs at each position in the three data sets. For plotting purposes, the frequencies were smoothed using a running mean of 50 nt.

Sequences were extracted for intronic (300-nt) and exonic (50-nt) regions flanking the 5′ and 3′ splice sites of alternatively spliced cassette exons. In order to construct motif maps, the frequencies of the CISBP-RNA motif (38) for the target RNA-binding protein (RBP) (e.g., PCBP1) in each set of cassette exons were computed at each position (nt −300 to +50 bracketing the 3′ splice sites and nt −50 to 300 bracketing 5′ splice sites). For plotting purposes, frequencies were smoothed over a running mean of 20 nt.

One-sided Fisher's exact tests with FDR correction were performed, and motifs with an adjusted *P* value of <0.05 were considered significantly enriched.

mRNA quantification and RT-PCR. Fetal liver RNA from E12.5 and E14.5 embryos was purified using TRIzol (15596026; Invitrogen). Quantitative reverse transcription-PCR (qRT-PCR) and alternative splicing RT-PCR were performed as described previously (43, 44). Alternative splicing RT-PCR primers and qRT-PCR primers are listed in Table 1.

Western blot analysis. Total cellular extracts prepared from the TRIzol fraction of the tissue/cell preparations were analyzed as described previously (44). The PCBP1 and PCBP2 antibodies were described previously (13).

Purification of Ter119$^+$ red blood cells. Mature erythrocytes and erythroid precursor cells were purified from fetal livers by using Anti-Ter-119 microbeads according to the manufacturer's instructions (catalog no. 130-049-901, magnetically activated cell sorting [MACS]; Miltenyi Biotec, Inc.).

Statistics. Statistical significance (*P* values) between paired data sets was determined using two-tailed, unpaired Student's *t* test.

Software availability. Detailed information about the availability and versions of software used for the bioinformatics analysis is provided in Table S1 in the supplemental material.

Accession number(s). All sequencing data generated in this study have been deposited in the Gene Expression Omnibus (GEO) database under accession no. GSE178247 (available at http://www.ncbi.nlm.nih.gov/geo/).

SUPPLEMENTAL MATERIAL

Supplemental material is available online only.

SUPPLEMENTAL FILE 1, XLSX file, 0.01 MB.
SUPPLEMENTAL FILE 2, XLSX file, 0.6 MB.
SUPPLEMENTAL FILE 3, XLSX file, 0.3 MB.
SUPPLEMENTAL FILE 4, XLSX file, 0.1 MB.
SUPPLEMENTAL FILE 5, XLSX file, 0.1 MB.
SUPPLEMENTAL FILE 6, XLSX file, 0.2 MB.
SUPPLEMENTAL FILE 7, XLSX file, 0.1 MB.
SUPPLEMENTAL FILE 8, XLSX file, 0.1 MB.

ACKNOWLEDGMENTS

The authors appreciate the generosity of Liebhaber laboratory members for sharing various reagents and thoughts. We thank Daphne Yang, and Gayatri M. Schur for their help with several of the experiments.

This work was supported by a National Institutes of Health grant (MERIT grant R01HL065449 to S.A.L.). The work of Y.B. and A.J. was supported by grant R01GM128096 to Y.B.

X.J. and S.A.L. conceptualized the study, designed the experiments, and supervised the study. X.J., J.H., L.R.G., A.K., and C.D.-L. performed the experiments. E.T. aided in isolation of hematopoietic progenitors under the supervision of M.J.W. A.J. performed the bioinformatics analysis under the supervision of Y.B. X.J., A.J., and S.A.L. wrote the paper.

We declare that we have no conflicts of interest.

REFERENCES

1. Liebhaber SA. 1997. mRNA stability and the control of gene expression. Nucleic Acids Symp Ser 1997:29–32.
2. Waggoner SA, Liebhaber SA. 2003. Regulation of alpha-globin mRNA stability. Exp Biol Med (Maywood) 228:387–395. https://doi.org/10.1177/153537020322800409.
3. Russell JE, Morales J, Liebhaber SA. 1997. The role of mRNA stability in the control of globin gene expression. Prog Nucleic Acids Res Mol Biol 57:249–287. https://doi.org/10.1016/s0079-6603(08)60283-4.
4. Weiss IM, Liebhaber SA. 1994. Erythroid cell-specific determinants of alpha-globin mRNA stability. Mol Cell Biol 14:8123–8132. https://doi.org/10.1128/MCB.14.12.8123.
5. Weiss IM, Liebhaber SA. 1995. Erythroid cell-specific mRNA stability elements in the alpha 2-globin 3′ nontranslated region. Mol Cell Biol 15:2457–2465. https://doi.org/10.1128/MCB.15.5.2457.
6. Waggoner SA, Liebhaber SA. 2003. Identification of mRNAs associated with alphaCP2-containing RNP complexes. Mol Cell Biol 23:7055–7067. https://doi.org/10.1128/MCB.23.19.7055-7067.2003.
7. Holcik M, Liebhaber SA. 1997. Four highly stable eukaryotic mRNAs assemble 3′ untranslated region RNA-protein complexes sharing cis and trans components. Proc Natl Acad Sci U S A 94:2410–2414. https://doi.org/10.1073/pnas.94.6.2410.
8. Ji X, Kong J, Liebhaber SA. 2011. An RNA-protein complex links enhanced nuclear 3′ processing with cytoplasmic mRNA stabilization. EMBO J 30:2622–2633. https://doi.org/10.1038/emboj.2011.171.
9. Ji X, Kong J, Carstens RP, Liebhaber SA. 2007. The 3′ untranslated region complex involved in stabilization of human alpha-globin mRNA assembles in the nucleus and serves an independent role as a splice enhancer. Mol Cell Biol 27:3290–3302. https://doi.org/10.1128/MCB.02289-05.
10. Ji X, Kong J, Liebhaber SA. 2003. In vivo association of the stability control protein alphaCP with actively translating mRNAs. Mol Cell Biol 23:899–907. https://doi.org/10.1128/MCB.23.3.899-907.2003.
11. Ji X, Park JW, Bahrami-Samani E, Lin L, Duncan-Lewis C, Pherribo G, Xing Y, Liebhaber SA. 2016. alphaCP binding to a cytosine-rich subset of polypyrimidine tracts drives a novel pathway of cassette exon splicing in the mammalian transcriptome. Nucleic Acids Res 44:2283–2297. https://doi.org/10.1093/nar/gkw088.
12. Ji X, Wan J, Vishnu M, Xing Y, Liebhaber SA. 2013. alphaCP poly(C) binding proteins act as global regulators of alternative polyadenylation. Mol Cell Biol 33:2560–2573. https://doi.org/10.1128/MCB.01380-12.
13. Chkheidze AN, Lyakhov DL, Makeyev AV, Morales J, Kong J, Liebhaber SA. 1999. Assembly of the alpha-globin mRNA stability complex reflects binary interaction between the pyrimidine-rich 3′ untranslated region determinant and poly(C) binding protein alphaCP. Mol Cell Biol 19:4572–4581. https://doi.org/10.1128/MCB.19.7.4572.
14. Makeyev AV, Chkheidze AN, Liebhaber SA. 1999. A set of highly conserved RNA-binding proteins, alphaCP-1 and alphaCP-2, implicated in mRNA stabilization, are coexpressed from an intronless gene and its intron-containing paralog. J Biol Chem 274:24849–24857. https://doi.org/10.1074/jbc.274.35.24849.
15. Makeyev AV, Eastmond DL, Liebhaber SA. 2002. Targeting a KH-domain protein with RNA decoys. RNA 8:1160–1173. https://doi.org/10.1017/s135583820202808x.
16. Makeyev AV, Liebhaber SA. 2000. Identification of two novel mammalian genes establishes a subfamily of KH-domain RNA-binding proteins. Genomics 67:301–316. https://doi.org/10.1006/geno.2000.6244.
17. Makeyev AV, Liebhaber SA. 2002. The poly(C)-binding proteins: a multiplicity of functions and a search for mechanisms. RNA 8:265–278. https://doi.org/10.1017/s1355838202024627.
18. Charroux B, Angelats C, Fasano L, Kerridge S, Vola C. 1999. The levels of the bancal product, a Drosophila homologue of vertebrate hnRNP K protein, affect cell proliferation and apoptosis in imaginal disc cells. Mol Cell Biol 19:7846–7856. https://doi.org/10.1128/MCB.19.11.7846.
19. Colaiacovo MP, Stanfield GM, Reddy KC, Reinke V, Kim SK, Villeneuve AM. 2002. A targeted RNAi screen for genes involved in chromosome morphogenesis and nuclear organization in the Caenorhabditis elegans germline. Genetics 162:113–128. https://doi.org/10.1093/genetics/162.1.113.
20. Geng C, Macdonald PM. 2007. Identification of genes that influence gurken expression. Fly (Austin) 1:259–267. https://doi.org/10.4161/fly.5246.
21. Ghanem LR, Kromer A, Silverman IM, Chatterji P, Traxler E, Penzo-Mendez A, Weiss MJ, Stanger BZ, Liebhaber SA. 2016. The poly(C) binding protein Pcbp2, and its retrotransposed derivative Pcbp1, are independently essential to mouse development. Mol Cell Biol 36:304–319. https://doi.org/10.1128/MCB.00936-15.
22. Heinrich AC, Pelanda R, Klingmuller U. 2004. A mouse model for visualization and conditional mutations in the erythroid lineage. Blood 104:659–666. https://doi.org/10.1182/blood-2003-05-1442.
23. Wu H, Liu X, Jaenisch R, Lodish HF. 1995. Generation of committed erythroid BFU-E and CFU-E progenitors does not require erythropoietin or the erythropoietin receptor. Cell 83:59–67. https://doi.org/10.1016/0092-8674(95)90234-1.
24. Friend C, Scher W, Holland JG, Sato T. 1971. Hemoglobin synthesis in murine virus-induced leukemic cells in vitro: stimulation of erythroid differentiation by dimethyl sulfoxide. Proc Natl Acad Sci U S A 68:378–382. https://doi.org/10.1073/pnas.68.2.378.
25. Kiledjian M, Wang X, Liebhaber SA. 1995. Identification of two KH domain proteins in the alpha-globin mRNP stability complex. EMBO J 14:4357–4364. https://doi.org/10.1002/j.1460-2075.1995.tb00110.x.
26. Ghanem LR, Kromer A, Silverman IM, Ji X, Gazzara M, Nguyen N, Aguilar G, Martinelli M, Barash Y, Liebhaber SA. 2018. Poly(C)-binding protein Pcbp2 enables differentiation of definitive erythropoiesis by directing functional splicing of the Runx1 transcript. Mol Cell Biol 38:e00175-18. https://doi.org/10.1128/MCB.00175-18.
27. Waggoner SA, Johannes GJ, Liebhaber SA. 2009. Depletion of the poly(C)-binding proteins alphaCP1 and alphaCP2 from K562 cells leads to p53-independent induction of cyclin-dependent kinase inhibitor (CDKN1A) and G1 arrest. J Biol Chem 284:9039–9049. https://doi.org/10.1074/jbc.M806986200.
28. Gamarnik AV, Andino R. 1997. Two functional complexes formed by KH domain containing proteins with the 5′ noncoding region of poliovirus RNA. RNA 3:882–892.
29. Tang YS, Khan RA, Zhang Y, Xiao S, Wang M, Hansen DK, Jayaram HN, Antony A. 2011. Incrimination of heterogeneous nuclear ribonucleoprotein E1 (hnRNP-E1) as a candidate sensor of physiological folate deficiency. J Biol Chem 286:39100–39115. https://doi.org/10.1074/jbc.M111.230938.
30. Ryu MS, Zhang D, Protchenko O, Shakoury-Elizeh M, Philpott CC. 2017. PCBP1 and NCOA4 regulate erythroid iron storage and heme biosynthesis. J Clin Invest 127:1786–1797. https://doi.org/10.1172/JCI90519.
31. Perrotti D, Calabretta B. 2002. Post-transcriptional mechanisms in BCR/ABL leukemogenesis: role of shuttling RNA-binding proteins. Oncogene 21:8577–8583. https://doi.org/10.1038/sj.onc.1206085.
32. Woolaway K, Asai K, Emili A, Cochrane A. 2007. hnRNP E1 and E2 have distinct roles in modulating HIV-1 gene expression. Retrovirology 4:28. https://doi.org/10.1186/1742-4690-4-28.
33. Chaudhury A, Hussey GS, Ray PS, Jin G, Fox PL, Howe PH. 2010. TGF-beta-mediated phosphorylation of hnRNP E1 induces EMT via transcript-selective

translational induction of Dab2 and ILEI. Nat Cell Biol 12:286–293. https://doi.org/10.1038/ncb2029.
34. Khandros E, Thom CS, D'Souza J, Weiss MJ. 2012. Integrated protein quality-control pathways regulate free α-globin in murine β-thalassemia. Blood 119:5265–5275. https://doi.org/10.1182/blood-2011-12-397729.
35. Zhang J, Socolovsky M, Gross AW, Lodish HF. 2003. Role of Ras signaling in erythroid differentiation of mouse fetal liver cells: functional analysis by a flow cytometry-based novel culture system. Blood 102:3938–3946. https://doi.org/10.1182/blood-2003-05-1479.
36. Pimkin M, Kossenkov AV, Mishra T, Morrissey CS, Wu W, Keller CA, Blobel GA, Lee D, Beer MA, Hardison RC, Weiss MJ. 2014. Divergent functions of hematopoietic transcription factors in lineage priming and differentiation during erythro-megakaryopoiesis. Genome Res 24:1932–1944. https://doi.org/10.1101/gr.164178.113.
37. An X, Schulz VP, Li J, Wu K, Liu J, Xue F, Hu J, Mohandas N, Gallagher PG. 2014. Global transcriptome analyses of human and murine terminal erythroid differentiation. Blood 123:3466–3477. https://doi.org/10.1182/blood-2014-01-548305.
38. Ray D, Kazan H, Cook KB, Weirauch MT, Najafabadi HS, Li X, Gueroussov S, Albu M, Zheng H, Yang A, Na H, Irimia M, Matzat LH, Dale RK, Smith SA, Yarosh CA, Kelly SM, Nabet B, Mecenas D, Li W, Laishram RS, Qiao M, Lipshitz HD, Piano F, Corbett AH, Carstens RP, Frey BJ, Anderson RA, Lynch KW, Penalva LOF, Lei EP, Fraser AG, Blencowe BJ, Morris QD, Hughes TR. 2013. A compendium of RNA-binding motifs for decoding gene regulation. Nature 499:172–177. https://doi.org/10.1038/nature12311.
39. Alvarez-Dominguez JR, Zhang X, Hu W. 2017. Widespread and dynamic translational control of red blood cell development. Blood 129:619–629. https://doi.org/10.1182/blood-2016-09-741835.
40. Heinicke LA, Nabet B, Shen S, Jiang P, van Zalen S, Cieply B, Russell JE, Xing Y, Carstens RP. 2013. The RNA binding protein RBM38 (RNPC1) regulates splicing during late erythroid differentiation. PLoS One 8:e78031. https://doi.org/10.1371/journal.pone.0078031.
41. Ulirsch JC, Nandakumar SK, Wang L, Giani FC, Zhang X, Rogov P, Melnikov A, McDonel P, Do R, Mikkelsen TS, Sankaran VG. 2016. Systematic functional dissection of common genetic variation affecting red blood cell traits. Cell 165:1530–1545. https://doi.org/10.1016/j.cell.2016.04.048.
42. Zhang J, Xu E, Ren C, Yan W, Zhang M, Chen M, Cardiff RD, Imai DM, Wisner E, Chen X. 2014. Mice deficient in Rbm38, a target of the p53 family, are susceptible to accelerated aging and spontaneous tumors. Proc Natl Acad Sci U S A 111:18637–18642. https://doi.org/10.1073/pnas.1415607112.
43. Ji X, Humenik J, Liebhaber SA. 2019. A cytosine-rich splice regulatory determinant enforces functional processing of the human α-globin gene transcript. Blood 133:2338–2347. https://doi.org/10.1182/blood-2018-12-891408.
44. Ji X, Humenik J, Yang D, Liebhaber SA. 2018. PolyC-binding proteins enhance expression of the CDK2 cell cycle regulatory protein via alternative splicing. Nucleic Acids Res 46:2030–2044. https://doi.org/10.1093/nar/gkx1255.
45. Chen MJ, Yokomizo T, Zeigler BM, Dzierzak E, Speck NA. 2009. Runx1 is required for the endothelial to haematopoietic cell transition but not thereafter. Nature 457:887–891. https://doi.org/10.1038/nature07619.
46. Okuda T, van Deursen J, Hiebert SW, Grosveld G, Downing JR. 1996. AML1, the target of multiple chromosomal translocations in human leukemia, is essential for normal fetal liver hematopoiesis. Cell 84:321–330. https://doi.org/10.1016/S0092-8674(00)80986-1.
47. Tober J, Maijenburg MW, Speck NA. 2016. Taking the leap: Runx1 in the formation of blood from endothelium. Curr Top Dev Biol 118:113–162. https://doi.org/10.1016/bs.ctdb.2016.01.008.
48. Wang Q, Stacy T, Binder M, Marin-Padilla M, Sharpe AH, Speck NA. 1996. Disruption of the Cbfa2 gene causes necrosis and hemorrhaging in the central nervous system and blocks definitive hematopoiesis. Proc Natl Acad Sci U S A 93:3444–3449. https://doi.org/10.1073/pnas.93.8.3444.
49. Conboy J, Kan YW, Shohet SB, Mohandas N. 1986. Molecular cloning of protein 4.1, a major structural element of the human erythrocyte membrane skeleton. Proc Natl Acad Sci U S A 83:9512–9516. https://doi.org/10.1073/pnas.83.24.9512.
50. Rana AP, Ruff P, Maalouf GJ, Speicher DW, Chishti AH. 1993. Cloning of human erythroid dematin reveals another member of the villin family. Proc Natl Acad Sci U S A 90:6651–6655. https://doi.org/10.1073/pnas.90.14.6651.
51. Siegel DL, Branton D. 1985. Partial purification and characterization of an actin-bundling protein, band 4.9, from human erythrocytes. J Cell Biol 100:775–785. https://doi.org/10.1083/jcb.100.3.775.
52. Conboy J, Mohandas N, Tchernia G, Kan YW. 1986. Molecular basis of hereditary elliptocytosis due to protein 4.1 deficiency. N Engl J Med 315:680–685. https://doi.org/10.1056/NEJM198609113151105.
53. Conboy JG, Chan J, Mohandas N, Kan YW. 1988. Multiple protein 4.1 isoforms produced by alternative splicing in human erythroid cells. Proc Natl Acad Sci U S A 85:9062–9065. https://doi.org/10.1073/pnas.85.23.9062.
54. Conboy JG, Chan JY, Chasis JA, Kan YW, Mohandas N. 1991. Tissue- and development-specific alternative RNA splicing regulates expression of multiple isoforms of erythroid membrane protein 4.1. J Biol Chem 266:8273–8280. https://doi.org/10.1016/S0021-9258(18)92973-X.
55. Huang SC, Zhang HS, Yu B, McMahon E, Nguyen DT, Yu FH, Ou AC, Ou JP, Benz EJ, Jr. 2017. Protein 4.1R exon 16 3′ splice site activation requires coordination among TIA1, Pcbp1, and RBM39 during terminal erythropoiesis. Mol Cell Biol 37:e00446-16. https://doi.org/10.1128/MCB.00446-16.
56. Ran FA, Hsu PD, Wright J, Agarwala V, Scott DA, Zhang F. 2013. Genome engineering using the CRISPR-Cas9 system. Nat Protoc 8:2281–2308. https://doi.org/10.1038/nprot.2013.143.
57. Doench JG, Fusi N, Sullender M, Hegde M, Vaimberg EW, Donovan KF, Smith I, Tothova Z, Wilen C, Orchard R, Virgin HW, Listgarten J, Root DE. 2016. Optimized sgRNA design to maximize activity and minimize off-target effects of CRISPR-Cas9. Nat Biotechnol 34:184–191. https://doi.org/10.1038/nbt.3437.
58. Vaquero-Garcia J, Barrera A, Gazzara MR, González-Vallinas J, Lahens NF, Hogenesch JB, Lynch KW, Barash Y. 2016. A new view of transcriptome complexity and regulation through the lens of local splicing variations. eLife 5:e11752. https://doi.org/10.7554/eLife.11752.
59. Bailey TL, Boden M, Buske FA, Frith M, Grant CE, Clementi L, Ren J, Li WW, Noble WS. 2009. MEME SUITE: tools for motif discovery and searching. Nucleic Acids Res 37:W202–W208. https://doi.org/10.1093/nar/gkp335.